First-principles screening of ABO$_3$ oxides with two magnetic sublattices

Hong Jian Zhao,[1,2] Laurent Bellaiche,[2] and Jorge Íñiguez[1,3]

[1]*Materials Research and Technology Department, Luxembourg Institute of Science and Technology (LIST),*
Avenue des Hauts-Fourneaux 5, L-4362 Esch/Alzette, Luxembourg

[2]*Physics Department and Institute for Nanoscience and Engineering, University of Arkansas, Fayetteville, Arkansas 72701, USA*

[3]*Physics and Materials Science Research Unit, University of Luxembourg, 41 Rue du Brill, L-4422 Belvaux, Luxembourg*

Work on orthoferrite perovskites (e.g., GdFeO$_3$) shows that ABO$_3$ oxides with A and B magnetic cations present novel behaviors (e.g., magnetoelectric) not possible when only one cation has spin. Unfortunately, the magnetic A cations are usually lanthanides whose $4f$ electrons interact weakly, restricting the most interesting effects to low temperatures. Here we explore the possibility of having both A and B sites occupied by $3d$ transition metals, by running a systematic first-principles investigation of 81 compositions, considering the polymorphs most likely to be stable in bulk or thin-film forms (perovskite, corundum derivatives). We predict specific compounds to be multiferroics at high temperature, multiferroics with large magnetic moments, "multiferroic metals" (i.e., as the much-sought "polar metals," but also magnetic), and ferromagnetic insulators. Our results offer a compelling panoramic of these compounds and the possibilities they offer, providing plenty of directions for further original research, both theoretical and experimental.

I. INTRODUCTION

Identifying new room-temperature magnetoelectric multiferroic materials (MEMs), combining both magnetism and ferroelectricity, has been a research priority for the past 15 years [1–3]. MEMs are unique in that their magnetic properties can be controlled by applied electric fields (and, conversely, magnetic fields act on their electric polarization and response), a possibility of great interest as regards the design of (low-power) devices for electronics and spintronics, data storage, and so on. Yet, most known MEMs present such appealing behaviors only at relatively low temperatures, BiFeO$_3$ [4] remaining the only simple, easy to prepare compound that is apt for room-temperature (T_{room}) applications.

Interestingly, Zhao *et al.* recently showed that, for ABO$_3$ compounds with two active magnetic sublattices, novel ferroelectric, and multiferroic effects can be expected to occur [5]. In the particular case studied by these authors, multiferroic GdFeO$_3$ [6], ferroelectricity results from a symmetry breaking caused by simple G-type antiferromagnetic (G-AFM) spin arrangements, characterized by antiparallel first-nearest-neighboring spins (see Fig. 1), adopted by both Gd and Fe spin sublattices. Similar effects were observed in the so-called type II multiferroic compounds [7], which display an improper ferroelectric order caused by the symmetry breaking in a magnetic transition. Yet the case of GdFeO$_3$ presents a key difference: Instead of the complex (cycloid, spiral) spin orders of typical type II multiferroics (e.g., TbMnO$_3$ [8]), here multiferroism relies on trivial AFM orders that are very frequent [9,10], suggesting that ABO$_3$ compounds with both A and B spin sublattices are, in principle, good candidates to yield MEMs via the mechanisms discussed in Ref. [5].

With this motivation, here we use first-principles methods to study an extensive collection of ABO$_3$ compounds

with A and B magnetic sublattices, characterizing their basic electronic, magnetic, and polar properties. We obtain some perovskite-like solutions that resemble the behavior of GdFeO$_3$ (e.g., potentially, perovskite films of FeNiO$_3$, which might constitute a high-temperature type II MEM). Yet, in the vast majority of cases our simulations yield nonperovskite structures that have, nevertheless, very interesting properties, even exceeding our expectations. For example, we predict a good number of strong proper ferroelectrics that are also magnetic, which renders them "type I" MEMs [7]. In particular, we have plausible predictions for room-temperature MEMs (e.g., CoFeO$_3$ and CrFeO$_3$, both with a LiNbO$_3$ structure) and MEMs with large magnetization (e.g., LiNbO$_3$-type ScTiO$_3$ and ScVO$_3$; perovskite TiCrO$_3$; perovskite films of MnCrO$_3$). Further, we also have more exotic predictions, such as "metallic multiferroics" (e.g., LiNbO$_3$-type NiCrO$_3$ and NiFeO$_3$) or ferromagnetic insulators (e.g., CrVO$_3$ and MnVO$_3$, both with the ilmenite structure). In the following we summarize our findings, giving some details on our most appealing results.

II. OUR APPROACH

Here we describe our approach as regards the selection of materials for our screening calculations, as well as the simulation methods employed.

A. Materials to screen

Currently known ABO$_3$ oxides with A and B magnetic sublattices often involve rare-earth lanthanide ions (denoted by R) at the A site. The spin-polarized electrons thus belong to a $4f$ shell very localized around the ionic core, and the corresponding spin-spin interactions are rather weak, which results in very low ordering temperatures. In contrast, the B
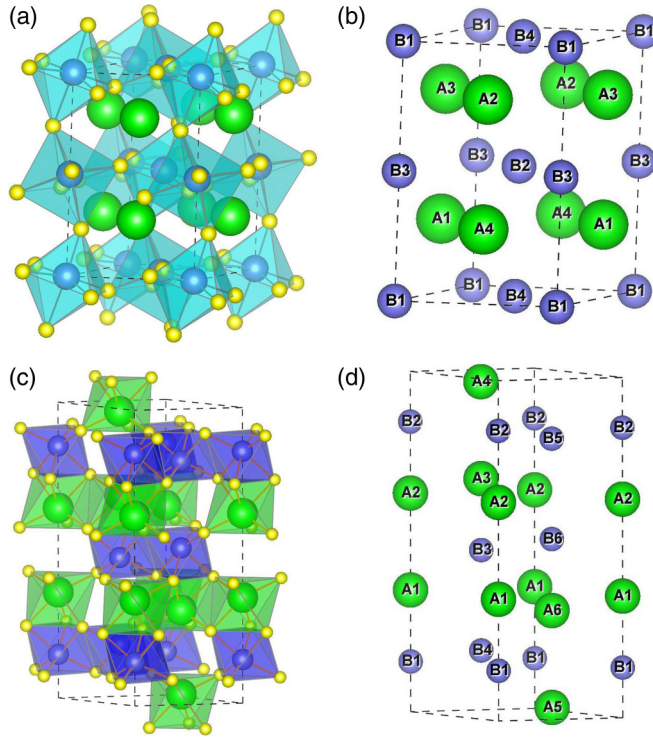
FIG. 1. Spin orders discussed in this work. (a), (b): Sketch of the perovskite (PK), LiNbO$_3$-type (LN-type), or Al$_2$O$_3$-like (AO-like) lattices (a), with the cations numbered in (b). The FM order corresponds to all spins being parallel, in both the A and B sublattices. The FiM order corresponds to having all A cations with spin up, and all B cations with spin down. The AFM1 order corresponds to having cations $A1$, $A2$, $B1$, and $B2$ with spin up, and all others with spin down. Finally, the AFM2 order corresponds to having the $A1$, $A2$, $B3$, and $B4$ cations with spin up, and all others with spin down. (c), (d): Sketch of the I lattice (c), with the cations numbered in (d). The FM and FiM orders are defined as above. The AFM1 order corresponds to having the $A1$, $A3$, $A5$, $B1$, $B3$, and $B5$ cations with spin up, and all others with spin down. The AFM2 order corresponds to having the $A1$, $A3$, $A5$, $B2$, $B4$, and $B6$ cations with spin up, and all others with spin down.

cations are usually first-row transition metals (TMs); their unpaired $3d$ electrons interact strongly via $B-\mathrm{O}-B$ super-exchange couplings that are dominant in insulating perovskite oxides, and ordering temperatures are relatively high [11]. For example, in GdFeO$_3$ the iron spins order at about 660 K, while the Gd spins order at about 2.5 K [9]; this is the typical situation, obviously incompatible with observing at T_room the MEM behavior discussed in Ref. [5].

To obtain ABO$_3$ compounds with both A and B spin sub-lattices ordering at relatively high temperatures, one might try to replace the R-cations at the A-site by species featuring less-localized magnetic electrons. A natural possibility is to consider TMs, i.e., elements with partly filled $3d$, $4d$, or $5d$ shells. Then, since we are particularly interested in identifying MEMs, which must thus be insulators, it seems most reasonable to restrict ourselves to first-row TMs. Indeed, it is known that the more-delocalized $4d$ and $5d$ electrons tend to render metallic phases, while insulating states are more likely to occur for the less-spread $3d$ states. Hence, here we investigate
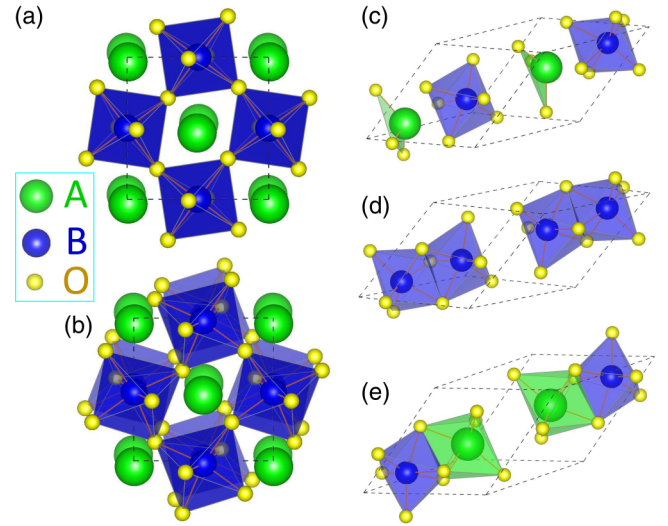

FIG. 2. Polymorphs obtained as lowest-energy solutions. (a) Perovskite lattice with a "$a^-a^-c^+$" pattern of rotations of the O$_6$ groups (symmetry *Pbnm*, see text), as it occurs in GdFeO$_3$; the view is along the axis of in-phase rotations. (b) Perovskite lattice with stronger "$a^-a^-c^+$" tilts, as it occurs, e.g., in TiCrO$_3$; a polar distortion, roughly perpendicular to the plane of the figure (i.e., along the axis of the c^+ rotations) reduces the symmetry to *Pna*2$_1$. (c) Perovskite lattice with "$a^-a^-a^-$" tilts and a polar distortion along the tilting axis (elongated direction of the shown cell), as it occurs in BiFeO$_3$ (*R*3*c* space group). When the tilts are very large, the A and B cations acquire similar octahedral oxygen environments, and we have a LiNbO$_3$-like lattice. (d) Corundum structure of Al$_2$O$_3$, which is essentially obtained from the LiNbO$_3$ lattice for same A and B cations. (e) Ilmenite structure, as that of FeTiO$_3$.

ABO$_3$ compounds in which both the A and B sites are occupied by a first-row transition metal, namely, Sc, Ti, V, Cr, Mn, Fe, Co, Ni, or Zn. We consider all possible combinations, which yields a total of 81 compositions.

Admittedly, ABO$_3$ perovskites with a first-row TM at the A site are not that common. Such cations (in typical 2+, 3+, or 4+ ionization states) all have relatively small ionic radii [12], and the few existing perovskites of this type (e.g., ScAlO$_3$ [13], ScVO$_3$ [14], double-perovskite Sc$_2$NiMnO$_6$ [15], as well as other In- and Mn-based compounds) can be obtained only by special synthesis routes [15]. Rather, small-A ABO$_3$ compounds tend to present other structures, as, for example, the so-called corundum-derivative phases [Figs. 2(c) to 2(e)]. For example, FeTiO$_3$ and MnTiO$_3$ usually crystallize in the nonpolar ilmenite (I) structure, and they can also be prepared as a LiNbO$_3$-type (LN-type) polymorph [16,17]. Note that, in the latter case, the polar order is proper (mimicking that of prototype one-dimensional ferroelectric LiNbO$_3$), which makes these materials type-I MEMs [7]. (Further, these particular compositions feature only one spin sublattice, as Ti^{4+} presents a nonmagnetic $3d^0$ electronic configuration.) Similarly, ScFeO$_3$ presents a metastable LN-phase that has been found to be a T_room MEM with weak magnetization [18]. Beyond the LN polar structure, Al$_2$O$_3$-like (AO-like, the original corundum structure in Fig. 2(d) [19]) configurations are also common among materials with the same cation occupying the A and B sites.

Other polymorphs occur frequently among ABO_3 compounds with small A cations. Thus, for example, $ScFeO_3$ presents the bixbyite structure at ambient conditions [18]; manganites like $ScMnO_3$ present a well-known hexagonal polymorph [20,21]. Interestingly, in many cases materials with these chemical formulas can be stabilized as LN- or I-type phases, using appropriate synthesis routes [15]. Further, the growth of thin films on appropriate substrates is another reportedly effective strategy to obtain metastable structures, in particular, perovskites. Examples include $YMnO_3$ [21] and $ScMnO_3$ [22], which present a nonperovskite hexagonal polymorph in bulk-like conditions. Hence, needing to define a tractable problem, here we restrict ourselves to the investigation of perovskite (PK) and corundum-related structures of small-A ABO_3 materials, as the literature suggests there should be reasonable chances of realizing experimentally our most promising predictions.

Having defined a broad and relevant space of possible compositions (81 ABO_3 compositions where both A and B are first-row TM atoms) and structures (most common PK phases, as well as LN-, AO-, and I-type polymorphs), we use first-principles methods to screen all the resulting materials, so as to identify the most promising candidates to present interesting functional properties. For each of the simulated structures, we considered the spin arrangements sketched in Fig. 1.

B. Simulation methods

For our simulations we use density functional theory within a generalized-gradient approximation adapted for solids (usually denoted "PBEsol" [23]) as implemented in the VASP package [24,25]. To better treat the strongly correlated $3d$ electrons, a "Hubbard-U" correction [26] with $U = 4$ eV is used throughout. The interactions between ionic cores and valence electrons are treated within the projector-augmented wave (PAW) formalism [27], solving the following electrons explicitly: $3s$, $3p$, $3d$, $4s$ for Sc; $3d$ and $4s$ for Ti, V, Cr, Mn, Fe, Co, Ni, and Zn; $2s$ and $2p$ for O. A plane-wave energy cutoff of 500 eV was used in all cases. For each oxide, we start from four initial structural phases: a tetragonal ferroelectric PK phase (like that of $BaTiO_3$), a rhombohedral ferroelectric PK phase (like that of $BiFeO_3$), an orthorhombic nonpolar PK phase (like that of $GdFeO_3$), and a characteristic I-type structure (like that of ilmenite $FeTiO_3$). The LN and AO solutions are obtained as a relaxation when we use the PK $BiFeO_3$-like structure as a starting point. A k-point mesh of $6 \times 6 \times 4$ is used for sampling the Brillouin zone of the orthorhombic PK polymorph, and similarly dense meshes are used for all other structures. Structural optimizations are carried out by relaxing both atomic positions and cell vectors; residual forces are below 0.01 eV/Å and residual stresses typically below 0.1 GPa. Electric polarizations were computing using the Berry-phase formalism [28]. Atomic magnetic moments were estimated from projections to localized orbitals employed within the PAW scheme, and are provided here as indicative of the basic electronic state of the cation.

We made extensive use of freely available crystallographic tools [29,30] to analyze the symmetry and distortions of our relaxed structures. We also used the VESTA [31] and MATPLOTLIB [32] packages for visualization of structures and data.

Let us discuss briefly our choice of Hubbard-corrected density functional theory (DFT + U) for this work. An intensive investigation like this one, which involves numerous structural optimizations for varying compositions and spin arrangements, requires a computationally light method for it to be feasible. Additionally, DFT + U simulations have been shown to yield qualitatively and semiquantitatively correct results for many multiferroic and related compounds, including ferrites [33,34], manganites [35,36], and even nickelates [37,38] displaying exotic charge- and orbital-ordering effects. Further, DFT + U has been used to compute the parameters of suitable spin Hamiltonians that can be solved numerically to yield magnetic-ordering temperatures in agreement with experiment [39,40]. Hence, DFT + U provides us with a practical simulation approach that should yield generally reliable results. Having said this, let us stress that one should not take our DFT + U results blindly. The treatment of the strongly correlated electrons in our compounds is not trivial, and DFT + U not infallible; thus, a detailed investigation of specific compounds would require a careful check of the computational approach being used.

Here, we tested the results for selected materials by repeating our calculations for alternative values of the U correction, namely, 3 and 5 eV. Generally speaking, our tests show that our essential results and conclusions are not U-dependent. For example, in the case of $ScVO_3$ (which poses the challenge of treating V^{3+} in the $3d^2$ configuration), we obtain the same lowest-energy polymorph for all U values considered, while the energy difference E^A–E^F between the lowest-lying antiferromagnetic and ferromagnetic orders ranges from 18 meV/f.u. (for $U = 3$ eV) to 11 meV/f.u. (for $U = 5$ eV). In other cases, such as $CoFeO_3$, the results for $U = 4$ eV and $U = 5$ eV are very similar (e.g., $E^A - E^F$ changes from -280 meV/f.u. to -255 meV/f.u.); yet, for $U = 3$ eV we obtain qualitatively different solutions: the Co cation adopts a low-spin configuration for some spin arrangements, while it is always in a high-spin state when larger U values are used in the calculation. Finally, let us note that some of our results—e.g., regarding the relative stability of different polymorphs—involve very tiny energy differences. In such cases, the choice of U, as well as other technicalities of the calculations (most notably, the density functional used [41,42]), can be expected to impact the qualitative outcome. Yet, our main conclusions are robust against this difficulty, as we are assuming from the start that special synthesis routes may be necessary to realize most of our materials predictions.

III. RESULTS

A. Screening calculations

As mentioned above, we consider all ABO_3 compositions where A and B are first-row TM elements (i.e., Sc, Ti, V, Cr, Mn, Fe, Co, Ni, Zn). For each composition, we relax the material starting from structures corresponding to all relevant polymorphs. These include two perovskite structures, i.e., the nonpolar orthorhombic phase of $CaTiO_3$ [$Pbnm$ space group, Fig. 2(a)] and the polar phase of $BiFeO_3$ [$R3c$ space group, Fig. 2(c)]. Note that the former structure becomes polar, with $Pca2_1$ symmetry, when both A and B sublattices

adopt the G-AFM spin order, as is the case of $GdFeO_3$ at low temperatures. As for the latter phase, it is characterized by antiphase O_6 rotations about the [111] pseudocubic axis—$a^-a^-a^-$ in Glazer's notation—and a proper ferroelectric polarization along that same direction. Interestingly, this $R3c$ phase can be viewed as a structural bridge between the PK and LN lattices [43]; indeed, all our calculations starting from $BiFeO_3$'s structure resulted in a relaxed solution that we identify with the LN-polymorph, with very large O_6 tilts exceeding 10°. (According to our calculations, $LiNbO_3$ and $BiFeO_3$ present O_6 rotations about the pseudocubic axes of about 13.7° and 8.1°, respectively.) Note that the LN structure yields the AO corundum phase mentioned above whenever the A and B sites are occupied by the same species. Finally, we also include the I-like polymorph [Fig. 2(e)]. In all cases, we consider the short-period spin arrangements shown in Fig. 1, which include the main ferromagnetic (FM) and AFM orders compatible with our studied polymorphs. This allows us to determine the dominant magnetic interactions in the investigated compounds. Notably, the AFM arrangements can be ferrimagnetic (FiM) whenever anti-aligned A and B spins do not compensate, but render a zero net magnetization whenever there is an antiparallel spin order within the A and B sublattices.

Let us note that these compounds are not trivial for a first-principles treatment, as many of them possess strongly correlated electrons in partly occupied orbital groups. At the same time, we know that computationally efficient simulation schemes as those based on "Hubbard-corrected" density functional theory (DFT + U) [26,44] render an acceptable description of the ground state of most such oxides; certainly this is the case for Fe^{3+} ferrites and Cr^{3+} chromites [5,41], but DFT + U also works reasonably well for more challenging compounds such as Co^{3+} cobaltites [40,45] or Ni^{3+} nickelates [37,46]. Further, the most likely shortcoming of the DFT + U approximation is a well-known one: it may yield a metallic solution for compounds that are actually insulating due to a poor treatment of dynamical correlations. Here we treat all our materials at the same level of DFT + U theory, choosing a typical correction of $U = 4$ eV for all atomic species considered. While such a drastic choice seems appropriate for a materials-screening investigation like this one, and we are confident that this approximation does not affect our main conclusions, one should keep in mind that, obviously, a more detailed study of individual compounds would require a specific assessment of the theory to employ. Here, as regards obtaining converged and sound results in a computationally reliable way, our employed approach worked well for all considered compositions except two, $VCoO_3$ and $CoVO_3$, for which the electronic solutions were not fully converged and which are thus excluded from our presentation below.

B. Most stable polymorphs

Figure 3 summarizes our results for the relative stability of the structural polymorphs here considered. The energy of a certain polymorph corresponds to the most stable spin order. For any given composition, we take the value for the I solution (E_I) as zero of energy. We find that the I and LN (or AO) structures are generally dominant. Our calculations predict

correctly a number of expected I-type ($FeTiO_3$ [47], $MnTiO_3$ [48], $CoTiO_3$ [49]) and AO-type (α-Fe_2O_3 [50], Cr_2O_3, V_2O_3 or Ti_2O_3 [51]) ground states. In many cases we obtain nearly degenerate polymorphs, suggesting that different structures can be stabilized via different synthesis routes. For example, for $ScFeO_3$ we obtain that the LN and PK polymorphs are nearly degenerate, with a slight preference for the former; this resonates with the experimental observation, i.e., that the PK phase can be reached from the bixbyite ground state upon heating and compressing, to later obtain a LN structure when the material is brought to ambient conditions [18].

It is interesting to note that the corundum-derived structures are characterized by a similar oxygen environment for both A and B cations, as both are caged in (distorted) O_6 octahedra. Since here we are considering materials with A and B cations of similar size, it is most natural that such corundum-type polymorphs dominate. As can be appreciated in Figs. 2(c) and 2(e), the difference between the LN and I polymorphs lies on the stacking of O_6 octahedra along the direction of the three-fold axis. Figure 2(c) also shows the cation off-centering responsible for the development of a ferroelectric (FE) polarization in the LN lattice. The polar LN phase has the $R3c$ space group, while the corresponding paraelectric (PE) structure would present the $R\bar{3}c$ symmetry. Interestingly, for all the materials studied in this work, the relaxation of the LN-type structure results in a polar phase, the PE structure always being a saddle point of the energy. (An exception to this rule happens whenever the A and B cations are the same; then we have a centrosymmetric AO-type phase instead of the FE LN-type polymorph.) For an illuminating discussion of corundum structures and their FE properties, we refer the reader to the works of Ye and Vanderbilt [52,53].

According to our simulations, only a few compositions display a PK ground state. Interestingly, a dominant PK solution is obtained mostly for compounds with Sc at the A or B sites; further, we obtain that the most likely PK structure is the $Pbnm$ orthorhombic phase of $CaTiO_3$, as consistent with the known general trends in the family [54,55]. Further, most of our PK structures are characterized by very large rotations of the O_6 octahedra: we typically obtain values of about 15°, quite larger than the angles ($\sim$12°) in compounds like $GdFeO_3$ [56]. A limit case is given by Zn_2O_3, where the tilts in the $a^-a^-c^+$ pattern are so large that the resulting structure can hardly be identified as a perovskite. (In fact, the ideal PK phase stops making sense as a reference structure for Zn_2O_3, which prevents us from quantifying the tilt amplitudes.) Thus, in the same way that a strongly tilted $a^-a^-a^-$ $BiFeO_3$-like structure takes us from the PK to the LN lattice, our results for Zn_2O_3 hint at the possibility of obtaining a new polymorph by exaggerating the $a^-a^-c^+$ tilts that are typical of $GdFeO_3$. We are not aware of any experimental realization of such a structure.

Finally, we also find that $TiCrO_3$ is a PK with an orthorhombic phase, but strongly polar in this case [Fig. 2(b)]. The corresponding space group is $Pna2_1$, and the resulting structure resembles that of $BiInO_3$ [57]. Interestingly, a less-distorted version of this phase (with smaller tilts and more regular O_6 octahedra) has been reported for $BiFeO_3$ [41] and $BiFeO_3$-$LaFeO_3$ solid solutions [58]. Note that this polar phase has exactly the same symmetry as that of $GdFeO_3$.
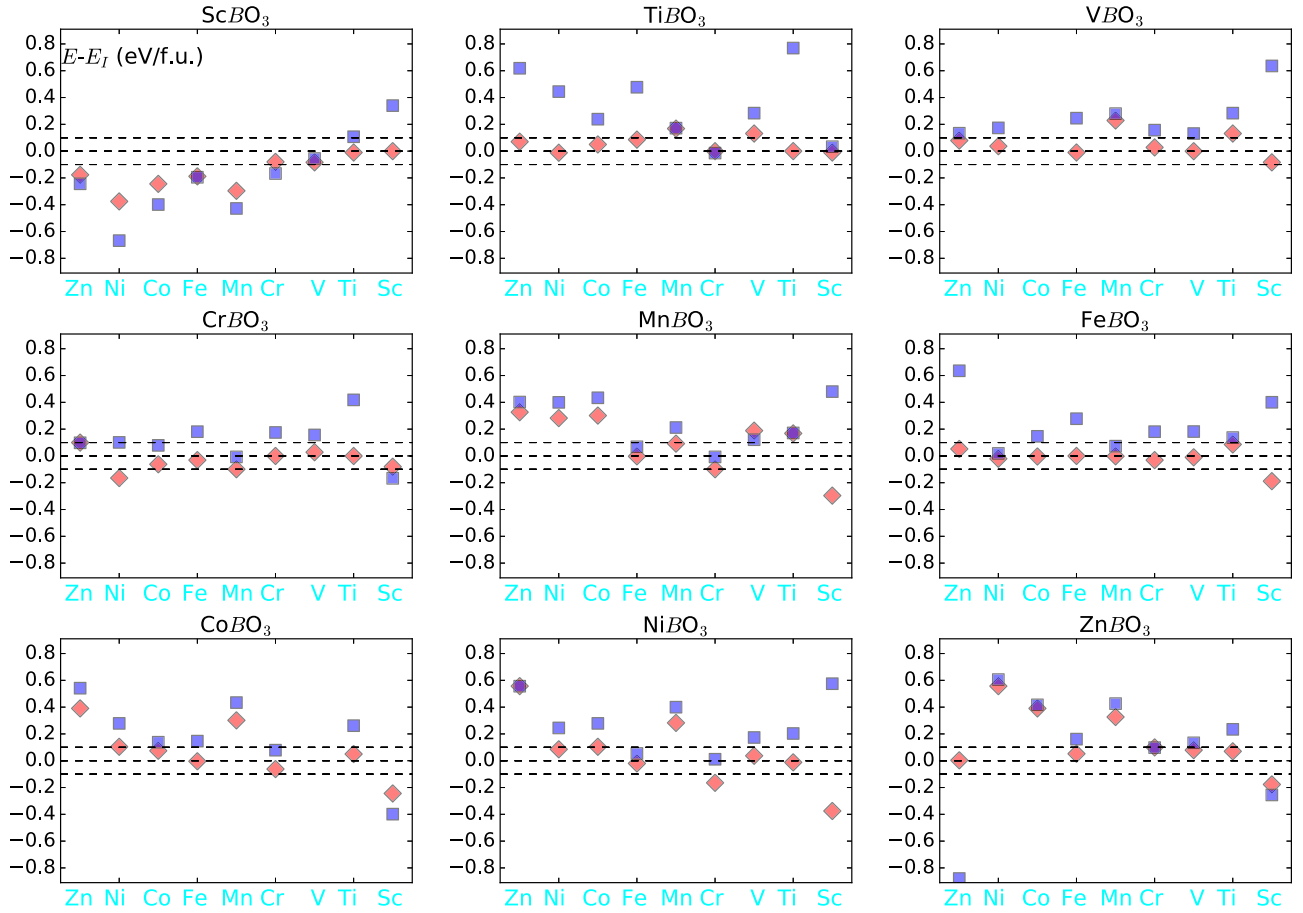
FIG. 3. Energies of the PK, LN (or AO), and I (taken as reference) structures of all the considered materials, given in eV *per* formula unit (f.u.). Blue squares and red diamonds correspond to PK and LN (or AO) solutions, respectively. For each composition and structure, we retain the energy corresponding to the most stable spin configuration.

However, in GdFeO$_3$ the polarization is improper and appears as a consequence of the symmetry breaking associated to the spin order; in contrast, TiCrO$_3$ is a proper ferroelectric, and thus a type I MEM. Admittedly, we did not expect to find a strongly ferroelectric ground state for TiCrO$_3$; yet it occurred naturally, as the result of a structural relaxation starting from a $Pna2_1$ GdFeO$_3$-like structure.

C. Functional properties

Figure 4 and Table I summarize our results as regards the functional properties of the most-stable polymorphs obtained. As shown in Fig. 4, most of the considered materials are predicted to be insulating, a result that we deem reliable given that our DFT + U methodology is a generally trustable theory to determine the insulating or metallic character of transition-metal oxides. (It goes without saying that particularly difficult cases, or a more accurate quantification of band gaps and other electronic features, may require higher-level theories.) Further, many of these insulating solutions present the polar LN structure and are thus, presumably, ferroelectric. (From our results, we cannot assure that these materials will have a switchable FE polarization; yet, we know they do comply with the necessary—and typically sufficient—requirements concerning symmetry and insulating character, which makes

them likely ferroelectrics.) We thus have many predictions for promising type I MEM behavior. In the following we give a brief account of our most remarkable results, as grouped in the categories of Fig. 4(a).

1. High-temperature multiferroics

Among the obtained insulating and FE compounds, some present strong AFM interactions. This is hardly a surprise, as AFM-type super-exchange couplings are dominant among insulating oxides. Hence, we find good candidates to display high-temperature magnetoelectric multiferroic behavior.

Table I lists the compounds that, according to our calculations, might be high-temperature MEMs. In the Table we give some details about the computed band gap, basic magnetic properties, and electric polarization of the three most promising ones, namely, CoFeO$_3$, CrFeO$_3$, and VFeO$_3$. In Fig. 5(a) we also show the computed density of states (DOS) of CoFeO$_3$, which is a representative case. It is interesting to note that the obtained energy difference between a FM spin arrangement and the AFM ground state ranges between 86 meV/f.u. for VFeO$_3$ to 280 meV/f.u. for CoFeO$_3$. This is in the range of values obtained for compounds like BiFeO$_3$ or GdFeO$_3$ (∼225 meV/f.u. [40]), which present Nèel temperatures above 600 K [9,59]. Hence, our screening
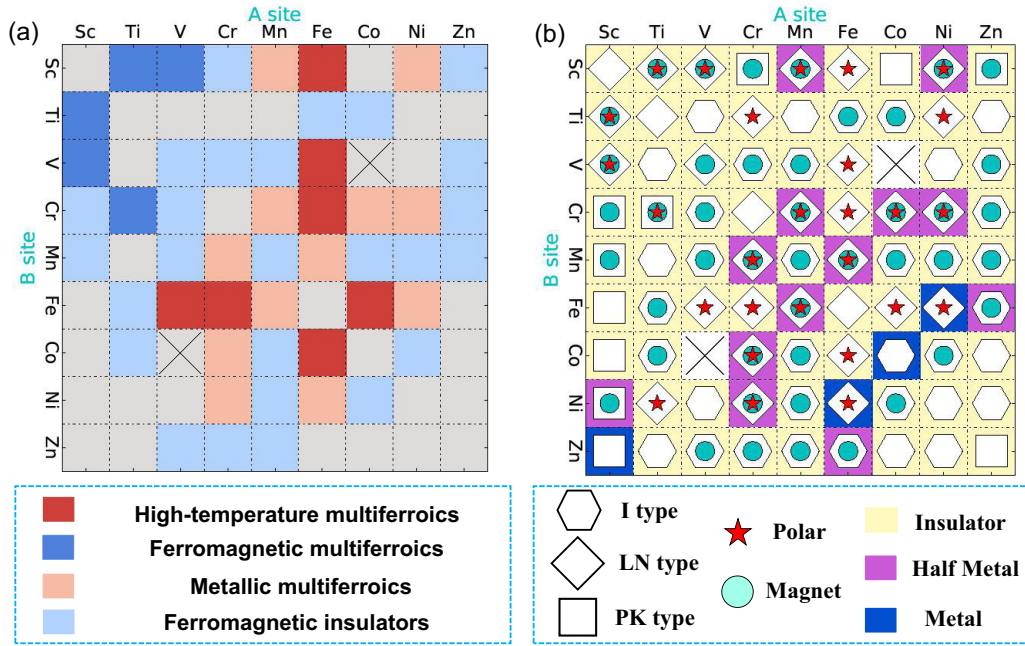
FIG. 4. Summary of our results. Panel (a) shows the materials that are predicted to present the most interesting properties, grouped in the four indicated categories. Panel (b) gives further detail on the most stable solutions obtained for each of the investigated compositions. As shown in the legend, we indicate the lowest-energy polymorph (PK-, LN-, or I-type), whether it is polar, whether it presents a net magnetization, and whether it is an insulator or (half)metal. Note that, whenever we have an LN-type solution with same A and B cations, it actually reduces to the AO corundum structure. Note that, because the A and B sites are crystallographically rather similar in the dominant corundum-like structures, this figure is approximately symmetric upon A–B swapping.

calculations suggest that these materials will be high- (even room-) temperature MEMs.

It is worth to note that, if we swap the A and B cations of the compounds just mentioned, the resulting materials (FeCoO$_3$, FeCrO$_3$, and FeVO$_3$) are all predicted to be LN-type insulators with AFM order. This suggests that the properties of these crystals will be robust against anti-site defects involving the A and B sublattices.

Another interesting compound in this category is FeScO$_3$, which is also predicted to be a LN-type insulator with an energy difference of 187 meV/f.u. between the FM spin arrangement and the AFM ground state. This ferrite is thus another candidate to be a T_{room} MFM, yet with only one magnetic sublattice in this case.

2. Multiferroics with large magnetization

All the above compounds are antiferromagnets with spin sublattices that perfectly cancel each other (AFM1 and AFM2 in Fig. 1). In such cases, the net magnetization will be either zero or very small, the latter possibility being associated to a small spin canting (not considered here).

Yet, we also find compounds whose lowest-energy phase is an insulating LN-type structure with a ferromagnetic ground state. The most interesting materials in this category are ScTiO$_3$ and ScVO$_3$, Fig. 5(b) showing a representative DOS result for the latter. In these compounds, the magnetic cations are Ti^{3+} and V^{3+}, respectively, and the FM interactions are associated to B–O–B superexchange paths forming relatively small angles [11]; for example, we obtain 134.6° for ScTiO$_3$. Interestingly, we find that the related compounds TiScO$_3$ and

VScO$_3$ have similar properties, which suggests that an experimental realization of these materials will be robust against antisite defects.

Thus, these materials are predicted to be MEMs with a large remnant magnetic moment, and are likely to attract great interest in the multiferroics community. Unfortunately, our calculations also suggest that the corresponding magnetic ordering temperatures will be quite low. As detailed in Table I, in this case the energy differences between relevant spin arrangements are of the order of 10 meV/f.u., which suggests Curie points well below T_{room}.

Finally, TiCrO$_3$ is a unique case that also falls within this category. As mentioned above, this compound is among the few predicted to present a PK-like ground state; in fact, a polar one with $Pna2_1$ space group [see Fig. 2(b)]. Further, it displays a lowest-energy FM configuration, separated by a sizable energy gap of 36 meV/f.u. from the most favorable AFM spin arrangement. Hence, we predict TiCrO$_3$ to be a FM MEM at moderately high temperatures, although most likely below T_{room}.

3. Metallic multiferroics

In addition to the many insulating solutions obtained, we also get a number of metals and half-metals (Fig. 4). In many cases, these metals present a polar LN structure, which automatically renders them "multiferroic metals." Today, there is great interest in identifying noncentrosymmetric (symmetry-wise polar) metals, which have been argued to display many interesting properties, ranging from higher superconductive temperatures to intrinsic Rashba effects [60–62]. Here, we

TABLE I. Most promising materials, and a brief summary of their properties. E^A is the energy of the lowest-lying AFM spin structure with a vanishing net magnetization (strictly zero within the colinear-spins approximation considered in this work), while E^F is the energy of the most stable spin order with a large net magnetization (FM or FiM). Energies ($E^A - E^F$), atomic magnetic moments (M) polarizations (P) and band gaps (E_{gap}) are given in meV/f.u., Bohr magnetons (μ_B), μC/cm^2 and eV, respectively. All LN, AO, and I structures present the $R3c$, $R\bar{3}c$, and $R\bar{3}$ space groups, respectively. PK polymorphs can present either the high-symmetry $Pbnm$ (e.g., typically the case of materials with a single magnetic sublattice, like ScCrO$_3$, labeled as "PK-$Pbnm$") or the reduced-symmetry $Pna2_1$ space group. Among the latter, the symmetry breaking can be either caused by the ordering of the two spin sublattices [e.g., FeNiO$_3$, labeled as "PK-$Pna2_1(1)$"] or by a proper polar distortion [e.g., TiCrO$_3$, labeled as "PK-$Pna2_1(2)$"]. Typically, we indicate the polymorph found to be most stable among those considered; solutions corresponding to a competing higher-energy polymorph are marked with an asterisk. Note that the ionization state of most cations can be inferred from the computed magnetic moments. For example, we obtain a value around 4 for Fe^{3+} in a high-spin configuration, which is typical of the projection method used here (see Methods). Similarly, for Cr^{3+} in a high-spin configuration we get $M_{Cr} \approx 3$, for high-spin Mn^{3+} we get values around 4, and so on.

	High-T multiferroics
CoFeO$_3$	LN-type, AFM with $E^A - E^F = -280$, $M_{Co} = 2.97$, $M_{Fe} = 4.11$, $P = 110$, $E_{gap} = 1.1$ eV
CrFeO$_3$	LN-type, AFM with $E^A - E^F = -92$, $M_{Cr} = 2.93$, $M_{Fe} = 4.16$, $P = 128$, $E_{gap} = 2.3$ eV
VFeO$_3$	LN-type, AFM with $E^A - E^F = -86$, $M_V = 1.90$, $M_{Fe} = 4.15$, $P = 122$, $E_{gap} = 1.8$ eV
FeNiO$_3$	PK-$Pna2_1(1)$ (*), AFM with $E^A - E^F = -108$, $M_{Fe} = 4.14$, $M_{Ni} = 0.82$, $P = 2.5$, $E_{gap} = 0.6$ eV
Other:	LN-type: FeCoO$_3$, FeCrO$_3$, FeVO$_3$, FeScO$_3$
	Multiferroics with large magnetization
ScTiO$_3$	LN-type, FM with $E^A - E^F = 7$, $M_{Ti} = 1.00$, Sc is not magnetic, $P = 91$, $E_{gap} = 2.0$ eV
ScVO$_3$	LN-type, FM with $E^A - E^F = 14$, $M_V = 2.00$, Sc is not magnetic, $P = 86$, $E_{gap} = 1.9$ eV
TiCrO$_3$	PK-$Pna2_1(2)$, FM with $E^A - E^F = 36$, $M_{Ti} = 1.04$, $M_{Cr} = 3.06$, $P = 44$, $E_{gap} = 1.7$ eV
MnCrO$_3$	PK-$Pna2_1(2)$ (*), FM with $E^A - E^F = 60$, $M_{Mn} = 4.03$, $M_{Cr} = 3.08$, $P = 58$, $E_{gap} = 0.2$ eV
Other:	LN-type: TiScO$_3$, VScO$_3$; PK-$Pna2_1(2)$ (*): CrMnO$_3$, MnCrO$_3$
	"Metallic multiferroics"
NiCrO$_3$	LN-type, FM half metal with $E^A - E^F = 305$, $M_{Ni} = 1.20$, $M_{Cr} = 2.98$
NiFeO$_3$	LN-type, AFM metal with $E^A - E^F = -32$, $M_{Ni} = 1.20$, $M_{Fe} = 4.06$
Other:	LN-type: CrNiO$_3$, CrMnO$_3$, MnCrO$_3$, MnScO$_3$, NiScO$_3$, CoCrO$_3$, CrCoO$_3$, MnFeO$_3$, FeMnO$_3$
	Ferromagnetic insulators
CrVO$_3$	I-type, FM with $E^A - E^F = 14$, $M_{Cr} = 3.08$, $M_V = 2.03$, $E_{gap} = 2.0$ eV
MnVO$_3$	I-type, FM with $E^A - E^F = 5$, $M_{Mn} = 4.54$, $M_V = 1.34$, $E_{gap} = 0.7$ eV
Other:	I-type: Mn$_2$O$_3$; PK-$Pbnm$: ScCrO$_3$, ScMnO$_3$

predict polar metals that are, in addition, magnetic. These could be interesting in various contexts, a notorious example being the quest for compounds presenting small skyrmions [63,64]: There, inversion-symmetry breaking is required to activate the spin-order interactions that cause noncollinear (skyrmion-like) spin arrangements, and the symmetry reduction is most usually achieved by introducing surfaces or interfaces; in our "multiferroic metals," inversion symmetry is intrinsically broken.

According to our results, compounds like NiCrO$_3$ or NiFeO$_3$ are promising "multiferroic metals." In particular, for NiCrO$_3$ we obtain relatively strong magnetic interactions that might yield this behavior even at T_{room}. The energy differences among relevant spin orders (most notably, 305 meV/f.u. in the case of NiCrO$_3$) are summarized in Table I. Figure 5(c) shows the computed DOS for the representative case of NiCrO$_3$, which features a clear half-metallic character.

As regards the amplitude of the polar distortion, these compounds are similar to the insulating LN-type polymorphs reported in Table I, which typically present spontaneous polarizations around 100 μC/cm^2. Yet, because NiCrO$_3$ and NiFeO$_3$ are metallic, their polarization is not defined and, thus, we do not report it in the table.

Finally, let us stress that the occurrence of structures that are simultaneously polar and metallic is not a surprise. While it is true that for years such solutions were deemed unlikely [65], today there is ample experimental [62] and theoretical [60,61] evidence that polarity (even ferroelectricity [66]) is compatible with metallicity and the attendant presence of free screening charges. In particular, whenever the polar distortion is driven by chemical or steric effects, metallicity does not affect much the polar distortion. This is the case of LiOsO$_3$ [62] or doped LiNbO$_3$ [60], where the small Li cation tends to move off from its high-symmetry position thus creating a polar distortion. The LN-like phases here studied, which all present a relatively small A cation, fall in the same category. Hence, our predictions of polar LN-type metals are compatible with our expectations from previous works on this problem.

4. Ferromagnetic insulators

Finally, let us briefly comment on the I-type solutions that we find. These compounds are nonpolar, and thus do not belong in any of the categories of multiferroics discussed above. Nevertheless, some of them present a rare and very
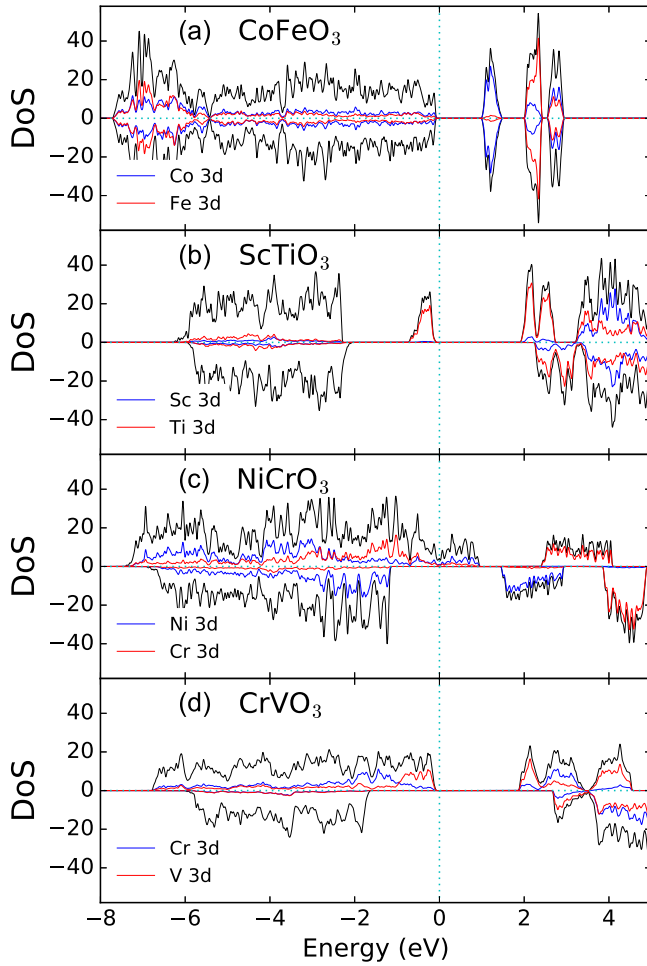
FIG. 5. Computed partial density of states of some of the materials highlighted in the text. (a) $CoFeO_3$, a candidate to be MEM at T_{room}. (b) $ScTiO_3$, a candidate to be MEM with large remnant magnetic moment. (c) $NiCrO_3$, a candidate to be a "multiferroic metal" at T_{room}. (d) $CrVO_3$, a prospective low-temperature ferromagnetic insulator.

interesting feature: they are simultaneously ferromagnetic and insulating.

As shown in Fig. 4 and Table I, our best materials in this category are $CrVO_3$, $MnVO_3$, and Mn_2O_3. Figure 5(e) shows the computed DOS of $CrVO_3$, as a representative case. Not surprisingly, in all cases the magnetic interactions are relatively small (never exceeding 20 meV/f.u.), which suggest relatively low ordering temperatures.

Interestingly, some of our PK solutions fall in this category as well. For example, our calculations predict that materials like $ScCrO_3$ and $ScMnO_3$ are insulators displaying a FM order at relatively low temperatures. As in the case of the FM LN-type compounds mentioned above, the ferromagnetism can be attributed to the large O_6 tilts, and relatively small B–O–B angles, occurring in these materials [11].

IV. DISCUSSION

Let us begin by noting that the results of Fig. 4 display an almost perfect symmetry upon swapping the A and B

sublattices. This makes good sense: While the A and B crystallographic sites are clearly different in the PK structure (in terms of oxygen coordination), the difference is not so marked in the LN- and I-type lattices. Hence, for LN- and I-type structures, ABO_3 and BAO_3 can be expected to be similar, but not necessarily identical; for perovskites, they can be expected to be quite different. Hence, since most of the obtained lowest-energy structures are either LN- or I-type, that explains the dominant (but not perfect) symmetry in Fig. 4.

Our materials screening yields other interesting results, beyond those cited above. For example, in addition to the high-T AFM MEMs (e.g., $CoFeO_3$) and low-T FM MEMs (e.g., $ScTiO_3$) cited in Table I, we obtain clear predictions for other, low-T MEMs with AFM spin order. LN-type compounds $NiTiO_3$ and $VFeO_3$ belong to that category.

We should also note that the above discussion is focused on the lowest-energy solutions obtained for the compositions considered. Yet, as is clear from Fig. 3, in many cases we find that the PK, LN, and I polymorphs lie very close in energy, which suggest that obtaining one or another may strongly depend on the experimental preparation conditions. See, for example, the remarkable case of $TiCrO_3$, for which we predict that these three polymorphs lie within a tiny 15 meV/f.u. energy window. With this in mind, we now briefly mention a number of appealing possibilities that involve metastable structures obtained in our investigation.

A notable case is that of of $FeNiO_3$. Here, while the predicted lowest-energy structure is a LN-type metal (Fig. 4), we have a low-lying insulating PK solution with $Pna2_1$ space group (Fig. 3). If it were possible to stabilize such a polymorph in thin-film form, e.g., by employing an appropriate PK as a substrate, we would be likely to obtain a type-II MEM analogous to $GdFeO_3$. (Note the relatively small polarization reported in Table I, which is characteristic of improper ferroelectric order in type-II MEMs.) Indeed, thin films of $FeNiO_3$ or other compositions displaying similar low-lying insulating PK phases (e.g., $MnVO_3$), may be our best hope to realize the MEM concept discussed in Ref. [5]—i.e., polar order driven by simple AFM orders in two spin sublattices—, which was our original motivation for this work. The $MnVO_3$ compound may be of particular interest, as in that case the PK structure is the polymorph lying immediately above the I-type ground state, which might facilitate obtaining it experimentally. (In contrast, for the mentioned $FeNiO_3$, the I-phase lies between the LN-type ground state and the PK polymorph.) On the negative side, the spin-ordering temperature for $MnVO_3$ is expected to be very low, as we obtain a tiny difference of 4 meV/f.u. between competing AFM and FM orders.

Additionally, many of our predicted I-type (nonpolar) materials present a low-lying LN-type (polar) polymorph that might be accessible by controlling the growth conditions, in an analogous way to what has been experimentally realized for $FeTiO_3$ and $MnTiO_3$ [16,17].

Let us also note the cases of $MnCrO_3$ and $CrMnO_3$. Our calculations predict these materials to display a LN-type ground state, with competitive I and PK phases. Interestingly, for the PK polymorph our simulations render the proper ferroelectric $Pna2_1$ structure that we predict to be the ground state of $TiCrO_3$. Hence, the growth of these compounds on a suitable PK substrates might render an interesting new

type of MEM with strong ferroelectricity and two magnetic sublattices. As a bonus, our calculations predict that the spin order in these compounds will be FM with a relatively high ordering temperature; most promisingly, for MnCrO$_3$ we obtain an energy difference between the FM and lowest-lying AFM states of 60 meV/f.u. in favor of the former.

On a different note, as regards the magnetic order, we have not been able to identify any clear trends across the family of compounds here considered. We have the impression that, to tackle this task, we need a better basic understanding of the factors determining the magnetic couplings in ABO$_3$ oxides with two different magnetic sublattices, a topic that is poorly investigated for PKs, let alone for LN- and I-type compounds.

Regarding magnetism, one may also wonder whether our results tell us something on how the transitions of the two magnetic sublattices will occur, e.g., together or separately. To explore this issue, let us consider the case of CrFeO$_3$, which is representative of the LN-type AFM multiferroics predicted in this work (see Table I). Let us postulate a simplest spin model, with only three independent exchange interactions (J_{CrCr}, J_{FeFe}, J_{CrFe}) connecting close neighbors, thus disregarding longer-range couplings and atomistic details (e.g., we assume a Cr atom sees eight equivalent Fe neighbors, which is not strictly the case in the LN structure). We can then compute such effective couplings by requesting this model reproduce the energies of three spin configurations considered in our screening calculations (AFM1, FM, and FiM in Fig. 1) plus an additional FiM order in which all Cr atoms are in the spin-up state while half of the Fe spins point up and half down. The obtained coupling constants are $J_{CrCr} = -0.2$ meV, $J_{FeFe} = -29.2$ meV, and $J_{FeCr} = -10.5$ meV, where the negative sign indicates an AFM interaction. These results suggest that the iron spins will order antiferromagnetically at a relatively high temperature. The Cr atoms will then be surrounded by four spin-up and four spin-down irons; thus, the strong J_{FeCr} couplings between individual Cr–Fe pairs will tend to cancel out, and the Cr spins will order at a relatively low temperature dictated by the weaker J_{CrCr} interaction. In sum, by considering some additional (simple) spin arrangements, we can supplement our screening calculations and make this sort of analysis for the investigated materials. However, this exercise does not allow us to test the validity of the very simple spin model postulated in this discussion, and the ensuing conclusions should thus be taken with a grain of salt. A reliable investigation would require a significant number of additional calculations to derive and validate a suitable spin Hamiltonian.

It is also interesting to comment on the electronic state of the A and B cations in our compounds. In our experience, the computed magnetic moments are the most informative quantity to estimate ionization states in these oxides, more reliable than approximate atomic-charge estimates. From the data in Table I, we find that the vast majority of our compounds present both A and B cations in a high-spin configuration corresponding to a 3+ ionization state. Thus, for example, for a compound like ScTiO$_3$ we obtain 1 unpaired spin for the Ti cation (corresponding to Ti^{3+}, or a $3d^1$ electronic configuration) and a null magnetic moment for Sc (corresponding to Sc^{3+} and a $3d^0$ electronic configuration). For example, for

MnCrO$_3$ we obtain four unpaired spins for Mn and three for Cr, which correspond to high-spin configurations $3d^4$ (Mn^{3+}) and $3d^3$ (Cr^{3+}), respectively. This kind of reasoning explains our results for most of compounds studies in this work.

The compounds with Ni are trickier, though. For example, according to the data in Table I, for NiCrO$_3$ we would say that we have a trivial Cr^{3+} in a high-spin state. That would imply that we have Ni^{3+} with a $3d^7$ electronic configuration; however, if that is the case, the result for the estimated magnetic moment (about 1.2 unpaired spins) is difficult to interpret. Indeed, if Ni^{3+} were in its frequent low-spin state, we should find one unpaired electron (or an even smaller moment, which would reflect a strong hybridization with surrounding oxygens); the other possible state of Ni^{3+}, with high spin, would present three unpaired electrons. The computed magnetic moment does not correspond to any of these limits, suggesting that a more careful analysis is needed to clarify the electronic states in this case. A detailed investigation of such difficult cases remains for future work.

Finally, let us comment on the thermodynamic stability of our predicted materials. If one looks at the experimentally synthesized ABO$_3$ compounds with a small transition metal A cation, essentially all of them are obtained by special synthesis routes, typically involving high pressures and/or temperatures [15]. This implies that the obtained compounds are thermodynamically metastable, the stable solution corresponding to a different polymorph or a phase separation into simpler oxides. For example, this is the case of the LN-phase of ScFeO$_3$, which was produced and characterized in Ref. [18], in spite of its tendency to phase separate; indeed, if, for example, we consider the lowest-energy solutions obtained in this work for Fe$_2$O$_3$ and Sc$_2$Fe$_3$, we obtain that the transformation 2ScFeO$_3 \rightarrow$ Fe$_2$O$_3$ + Sc$_2$O$_3$ is exothermic, with a released energy of about 0.29 eV. The situation is similar for other compounds predicted here and which have not been obtained experimentally yet. Thus, for example, our results indicate that the reaction 2ScCrO$_3 \rightarrow$ Sc$_2$O$_3$ + Cr$_2$O$_3$ has an energy reduction of 0.15 eV associated to it, while 2CrFeO$_2 \rightarrow$ Cr$_2$O$_3$ + Fe$_2$O$_3$ releases 0.12 eV. Hence, from a thermodynamic point of view, we have reasons to believe that the synthesis routes that make it possible to obtain materials like ScFeO$_3$ might also enable the synthesis of compounds like ScCrO$_3$ and CrFeO$_3$ as metastable phases. Similarly, as mentioned above for the cases of YMnO$_3$ and ScMnO$_3$, growth of thin films on suitable substrates is another much-employed strategy to stabilized metastable polymorphs of ABO$_3$ oxides, and a promising way to try to obtain the most interesting materials here predicted. Hence, in conclusion, most (if not all) our predicted compounds are expected to be metastable; yet, this fact does not lessen their interest.

V. CONCLUSION

We report on a computational screening of ABO$_3$ oxides in which both the A and B cations are first-row transition metals. Our calculations delivered a good number of predictions of great relevance to the fields of multiferroic and functional oxides. Most notably, we obtain new candidates to display magnetoelectric multiferroic properties, including room-temperature (antiferromagnetic) and lower-temperature

(ferro and ferrimagnetic) compounds. Further, we find a good number of high- (even room-) temperature "multiferroic metals," of potential interest for applications requiring a broken spatial inversion symmetry (from Rashba effects to skyrmions and photovoltaics). Finally, we obtain several insulating ferromagnets, albeit at relatively low temperatures, as well as a number of interesting metastable structures (e.g., ferromagnetic multiferroics with proper ferroelectricity) that might be grown as thin films on suitable substrates. While additional, more careful and material-specific, first-principles calculations may be required to better quantify and understand the properties of some of these compounds, our high-throughput investigation is detailed and reliable enough to reveal trends in the considered family and identify promising directions for further research. We thus hope our work will contribute to

invigorate the field of functional oxides, by broadening the range of materials types that can potentially present appealing physical properties and be useful for applications.

[1] M. Fiebig, Revival of the magnetoelectric effect, J. Phys. D **38**, R123 (2005).

[2] M. Fiebig, T. Lottermoser, D. Meier, and M. Trassin, The evolution of multiferroics, Nat. Rev. Mater. **1**, 16046 (2016).

[3] P. B. Meisenheimer, S. Novakov, N. M. Vu, and J. T. Heron, Perspective: Magnetoelectric switching in thin film multiferroic heterostructures, J. Appl. Phys. **123**, 240901 (2018).

[4] G. Catalan and J. F. Scott, Physics and applications of bismuth ferrite, Adv. Mater. **21**, 2463 (2009).

[5] H. J. Zhao, L. Bellaiche, X. M. Chen, and J. Íñiguez, Improper electric polarization in simple perovskite oxides with two magnetic sublattices, Nat. Commun. **8**, 14025 (2017).

[6] Y. Tokunaga *et al.*, Composite domain walls in a multiferroic perovskite ferrite, Nat. Mater. **8**, 558 (2009).

[7] D. Khomskii, Classifying multiferroics: Mechanisms and effects, Physics **2**, 20 (2009).

[8] T. Kimura *et al.*, Magnetic control of ferroelectric polarization, Nature **426**, 55 (2003).

[9] R. L. White, Review of recent work on the magnetic and spectroscopic properties of the rare-earth orthoferrites, J. Appl. Phys. **40**, 1061 (1969).

[10] E. Bousquet and A. Cano, Non-collinear magnetism in multiferroic perovskites, J. Phys.: Condens. Matter **28**, 123001 (2016).

[11] J. Goodenough, *Magnetism and the Chemical Bond*, (Interscience monographs on chemistry: Inorganic chemistry section) (Interscience, New York, 1963).

[12] R. D. Shannon, Revised effective ionic radii and systematic studies of interatomic distances in halides and chalcogenides, Acta Crystallogr., Sect. A **32**, 751 (1976).

[13] W. Sinclair, R. A. Eggleton, and A. E. Ringwood, Crystal synthesis and structure refinement of high-pressure $ScAlO_3$ perovskite, Z. Krist. - Cryst. Mater. **149**, 307 (2010).

[14] E. Castillo-Martínez, M. Bieringer, S. P. Shafi, L. M. D. Cranswick, and M. Á. Alario-Franco, Highly stable cooperative distortion in a weak Jahn-Teller d^2 cation: Perovskite-type $ScVO_3$ obtained by high-pressure and high-temperature transformation from bixbyite, J. Am. Chem. Soc. **133**, 8552 (2011).

[15] A. A. Belik and W. Yi, High-pressure synthesis, crystal chemistry and physics of perovskites with small cations at the A site, J. Phys.: Condens. Matter **26**, 163201 (2014).

[16] X. Wu, G. Steinle-Neumann, O. Narygina, C. McCammon, and L. Dubrovinsky, In situ high-pressure study of $LiNbO_3$-type $FeTiO_3$: X-ray diffraction and Mossbauer spectroscopy, High Press. Res. **30**, 395 (2010).

[17] N. L. Ross, J. Ko, and C. T. Prewitt, A new phase transition in $MnTiO_3$:$LiNbO_3$-perovskite structure, Phys. Chem. Miner. **16**, 621 (1989).

[18] T. Kawamoto *et al.*, Room-temperature polar ferromagnet $ScFeO_3$ transformed from a high-pressure orthorhombic perovskite phase, J. Am. Chem. Soc. **136**, 15291 (2014).

[19] E. N. Maslen, V. A. Streltsov, N. R. Streltsova, N. Ishizawa, and Y. Satow, Synchrotron x-ray study of the electron density in $\alpha - Al_2O_3$, Acta Crystallogr. Sect. B **49**, 973 (1993).

[20] F. Wang *et al.*, Abnormal magnetic ordering and ferromagnetism in perovskite $ScMnO_3$ film, Appl. Phys. Lett. **106**, 232906 (2015).

[21] P. A. Salvador, T.-D. Doan, B. Mercey, and B. Raveau, Stabilization of $YMnO_3$ in a perovskite structure as a thin film, Chem. Mater. **10**, 2592 (1998).

[22] J. Wang *et al.*, Negative-pressure-induced enhancement in a freestanding ferroelectric, Nat. Mater. **14**, 985 (2015).

[23] J. P. Perdew, A. Ruzsinszky, G. I. Csonka, O. A. Vydrov, G. E. Scuseria, L. A. Constantin, X. Zhou, and K. Burke, Restoring the Density-Gradient Expansion for Exchange in Solids and Surfaces, Phys. Rev. Lett. **100**, 136406 (2008).

[24] G. Kresse and J. Furthmüller, Efficient iterative schemes for *ab initio* total-energy calculations using a plane-wave basis set, Phys. Rev. B **54**, 11169 (1996).

[25] G. Kresse and D. Joubert, From ultrasoft pseudopotentials to the projector augmented-wave method, Phys. Rev. B **59**, 1758 (1999).

[26] S. L. Dudarev, G. A. Botton, S. Y. Savrasov, C. J. Humphreys, and A. P. Sutton, Electron-energy-loss spectra and the structural stability of nickel oxide: An LSDA+U study, Phys. Rev. B **57**, 1505 (1998).

[27] P. E. Blöchl, Projector augmented-wave method, Phys. Rev. B **50**, 17953 (1994).

[28] R. D. King-Smith and D. Vanderbilt, Theory of polarization of crystalline solids, Phys. Rev. B **47**, 1651 (1993).

[29] H. T. Stokes and D. M. Hatch, Findsym: Program for identifying the space-group symmetry of a crystal, J. Appl. Crystallogr. **38**, 237 (2005).

[30] D. Orobengoa, C. Capillas, M. I. Aroyo, and J. M. Perez-Mato, Amplimodes: Symmetry-mode analysis on the bilbao crystallographic server, J. Appl. Crystallogr. **42**, 820 (2009).

[31] K. Momma and F. Izumi, Vesta-3 for three-dimensional visualization of crystal, volumetric and morphology data, J. Appl. Crystallogr. **44**, 1272 (2011).

[32] J. D. Hunter, Matplotlib: A 2d graphics environment, Comput. Sci. Eng. **9**, 90 (2007).

[33] J. B. Neaton, C. Ederer, U. V. Waghmare, N. A. Spaldin, and K. M. Rabe, First-principles study of spontaneous polarization in multiferroic BiFeO$_3$, Phys. Rev. B **71**, 014113 (2005).

[34] A. Singh, V. N. Singh, E. Canadell, J. Íñiguez, and O. Diéguez, Polymorphism in Bi-based perovskite oxides: A first-principles study, Phys. Rev. Mater. **2**, 104417 (2018).

[35] C. J. Fennie and K. M. Rabe, Ferroelectric transition in YMnO$_3$ from first principles, Phys. Rev. B **72**, 100103(R) (2005).

[36] A. Malashevich and D. Vanderbilt, First Principles Study of Improper Ferroelectricity in TbMnO$_3$, Phys. Rev. Lett. **101**, 037210 (2008).

[37] J. Varignon, M. N. Grisolia, J. Íñiguez, A. Barthélémy, and M. Bibes, Complete phase diagram of rare-earth nickelates from first-principles, NPJ Quantum Materials **2**, 21 (2017).

[38] S. Catalano *et al.*, Rare-earth nickelates RNiO$_3$: Thin films and heterostructures, Rep. Prog. Phys. **81**, 046501 (2018).

[39] I. C. Infante, J. Juraszek, S. Fusil, B. Dupe, P. Gemeiner, O. Dieguez, F. Pailloux, S. Jouen, E. Jacquet, G. Geneste, J. Pacaud, J. Iniguez, L. Bellaiche, A. Barthelemy, B. Dkhil, and M. Bibes, Multiferroic Phase Transition Near Room Temperature in BiFeO_3 Films, Phys. Rev. Lett. **107**, 237601 (2011).

[40] O. Diéguez and J. Íñiguez, First-Principles Investigation of Morphotropic Transitions and Phase-Change Functional Responses in BiFeO$_3$ − BiCoO$_3$ Multiferroic Solid Solutions, Phys. Rev. Lett. **107**, 057601 (2011).

[41] O. Diéguez, O. E. González-Vázquez, J. C. Wojdeł, and J. Íñiguez, First-principles predictions of low-energy phases of multiferroic BiFeO$_3$, Phys. Rev. B **83**, 094105 (2011).

[42] O. Diéguez and J. Íñiguez, Epitaxial phases of BiMnO$_3$ from first principles, Phys. Rev. B **91**, 184113 (2015).

[43] T. Gu, T. Scarbrough, Y. Yang, J. Iniguez, L. Bellaiche, and H. J. Xiang, Cooperative Couplings between Octahedral Rotations and Ferroelectricity in Perovskites and Related Materials, Phys. Rev. Lett. **120**, 197602 (2018).

[44] V. I. Anisimov, F. Aryasetiawan, and A. I. Lichtenstein, First-principles calculations of the electronic structure and spectra of strongly correlated systems: The LDA+U method, J. Phys.: Condens. Matter **9**, 767 (1997).

[45] M. A. Korotin, S. Y. Ezhov, I. V. Solovyev, V. I. Anisimov, D. I. Khomskii, and G. A. Sawatzky, Intermediate-spin state and properties of LaCoO$_3$, Phys. Rev. B **54**, 5309 (1996).

[46] A. Mercy, J. Bieder, J. Íñiguez, and P. Ghosez, Structurally triggered metal-insulator transition in rare-earth nickelates, Nat. Commun. **8**, 1677 (2017).

[47] B. A. Wechsler and C. T. Prewitt, Crystal structure of ilmenite (FeTiO$_3$) at high temperature and high pressure, Am. Mineral. **69**, 176 (1984).

[48] R. H. Mitchell and R. P. Liferovic, The pyrophanite-ecandrewsite solid-solution: Crystal structures, of the Mn$_{1−x}$Zn$_x$SiO$_3$ series (0.1 $<= x <=$ 0.8), Can. Mineral. **42**, 1871 (2004).

[49] Y.-J. Lin, Y.-H. Chang, W.-D. Yang, and B.-S. Tsai, Synthesis and characterization of ilmenite NiTiO$_3$ and CoTiO$_3$ prepared by a modified pechini method, J. Non-Cryst. Solids **352**, 789 (2006).

[50] R. L. Blake, R. E. Hessevick, T. Zoltai, and L. W. Finger, Refinement of the hematite structure, Am. Mineral. **51**, 123 (1966).

[51] R. E. Newnham and Y. M. de Haan, Refinement of the alpha Al$_2$O$_3$, Ti$_2$O$_3$, V$_2$O$_3$ and Cr$_2$O$_3$ structures, Z. Krist. **117**, 235 (1962).

[52] M. Ye and D. Vanderbilt, Ferroelectricity in corundum derivatives, Phys. Rev. B **93**, 134303 (2016).

[53] M. Ye and D. Vanderbilt, Domain walls and ferroelectric reversal in corundum derivatives, Phys. Rev. B **95**, 014105 (2017).

[54] P. Chen, M. N. Grisolia, H. J. Zhao, O. E. Gonzalez-Vazquez, L. Bellaiche, M. Bibes, B. G. Liu, and J. Iniguez, Energetics of oxygen-octahedra rotations in perovskite oxides from first principles, Phys. Rev. B **97**, 024113 (2018).

[55] M. W. Lufaso and P. M. Woodward, Prediction of the crystal structures of perovskites using the software program *SPuDS*, Acta Crystallogr. Sect. B **57**, 725 (2001).

[56] S. Geller, Crystal structure of gadolinium orthoferrite, GdFeO$_3$, J. Chem. Phys. **24**, 1236 (1956).

[57] A. A. Belik, S. Y. Stefanovich, B. I. Lazoryak, and E. Takayama-Muromachi, BiInO$_3$: A polar oxide with gdfeo3-type perovskite structure, Chem. Mater. **18**, 1964 (2006).

[58] O. E. González-Vázquez, J. C. Wojdeł, O. Diéguez, and J. Íñiguez, First-principles investigation of the structural phases and enhanced response properties of the BiFeO$_3$ − LaFeO$_3$ multiferroic solid solution, Phys. Rev. B **85**, 064119 (2012).

[59] S. V. Kiselev, R. P. Ozerov, and G. S. Zhdanov, Detection of Magnetic Order in Ferroelectric BiFeO$_3$ by Neutron Diffraction, Soviet Physics Doklady **7**, 742 (1963).

[60] H. J. Zhao, A. Filippetti, C. Escorihuela-Sayalero, P. Delugas, E. Canadell, L. Bellaiche, V. Fiorentini, and J. Iniguez, Meta-screening and permanence of polar distortion in metallized ferroelectrics, Phys. Rev. B **97**, 054107 (2018).

[61] N. A. Benedek and T. Birol, "Ferroelectric" metals reexamined: Fundamental mechanisms and design considerations for new materials, J. Mater. Chem. C **4**, 4000 (2016).

[62] Y. Shi *et al.*, A ferroelectric-like structural transition in a metal, Nat. Mater. **12**, 1024 (2013).

[63] N. Nagaosa and Y. Tokura, Topological properties and dynamics of magnetic skyrmions, Nat. Nanotechnol. **8**, 899 (2013).

[64] S. Seki and M. Mochizuki, *Skyrmions in Magnetic Materials*. Springer Briefs in Physics (Springer International Publishing, New York, 2016).

[65] P. W. Anderson and E. I. Blount, Symmetry Considerations on Martensitic Transformations: "Ferroelectric" Metals? Phys. Rev. Lett. **14**, 217 (1965).

[66] A. Filippetti, V. Fiorentini, F. Ricci, P. Delugas, and J. Íñiguez, Prediction of a native ferroelectric metal, Nat. Commun. **7**, 11211 (2016).